

Article

Age and Geochemistry of Late Jurassic Mafic Volcanic Rocks in the Northwestern Erguna Block, Northeast China

Yan Li ^{1,2}, Feng-Jun Nie ^{1,*} and Zhao-Bin Yan ¹

¹ College of Earth Science, East China University of Technology, Nanchang 330013, China; 201800818002@ecut.edu.cn (Y.L.); zbyan@ecit.cn (Z.-B.Y.)

² No. 240 Institute of Nuclear Industry, The China National Nuclear Corporation, Shenyang 110000, China

* Correspondence: niefj@ecit.cn

Abstract: The northwestern Erguna Block, where a wide range of volcanic rocks are present, provides one of the foremost locations to investigate Mesozoic Paleo-Pacific and Mongol-Okhotsk subduction. The identification and study of Late Jurassic mafic volcanic rocks in the Badaguan area of northwestern Erguna is of particular significance for the investigation of volcanic magma sources and their compositional evolution. Detailed petrological, geochemical, and zircon U-Pb dating suggests that the Late Jurassic mafic volcanic rocks formed at 157–161 Ma. Furthermore, the geochemical signatures of these mafic volcanic rocks indicate that they are calc-alkaline or transitional series with weak peraluminous characteristics. The rocks have a strong MgO, Al₂O₃, and total alkali content, and a SiO₂ content of 53.55–63.68 wt %; they are enriched in Rb, Th, U, K, and light rare-earth elements (LREE), and depleted in high-field-strength elements (HFSE), similar to igneous rocks in subduction zones. These characteristics indicate that the Late Jurassic mafic volcanic rocks in the Badaguan area may be derived from the partial melting of the lithospheric mantle as it was metasomatized by subduction-related fluid and the possible incorporation of some subducting sediments. Subsequently, the fractional crystallization of Fe and Ti oxides occurred during magmatic evolution. Combined with the regional geological data, it is inferred that the studied mafic volcanic rocks were formed by lithospheric extension after the closure of the Mongol-Okhotsk Ocean.

Keywords: Late Jurassic mafic volcanic rocks; Erguna Block; Mongol-Okhotsk Ocean; age and geochemistry



check for updates

Citation: Li, Y.; Nie, F.-J.; Yan, Z.-B. Age and Geochemistry of Late Jurassic Mafic Volcanic Rocks in the Northwestern Erguna Block, Northeast China. *Minerals* **2021**, *11*, 1010. <https://doi.org/10.3390/min11091010>

Academic Editor: Jan C.M. De Hoog

Received: 28 July 2021

Accepted: 8 September 2021

Published: 17 September 2021

Publisher's Note: MDPI stays neutral with regard to jurisdictional claims in published maps and institutional affiliations.



Copyright: © 2021 by the authors. Licensee MDPI, Basel, Switzerland. This article is an open access article distributed under the terms and conditions of the Creative Commons Attribution (CC BY) license (<https://creativecommons.org/licenses/by/4.0/>).

1. Introduction

The northwestern margin of the Erguna Block underwent a complex tectonic evolution during the Phanerozoic, including ancient Asia, the Mongol-Okhotsk subduction, and the westward subduction of the Paleo-Pacific Ocean [1–5]. Multiple magmatic events resulted in the widespread distribution of igneous rocks in the northwestern Erguna Block [6–9]. The widely exposed igneous rocks provide a useful tool for reconstructing the tectonic evolution of this region and its surrounding areas. In recent years, with the increasing focus on the Mesozoic volcanic rocks in the Da Xing'anling region, a large amount of high-precision zircon U-Pb and ⁴⁰Ar/³⁹Ar age and geochemical data have been obtained. These data indicate that most of the Mesozoic volcanic rocks in the Da Xing'anling region formed during the Early Cretaceous [10,11], with most of the volcanic rocks consisting of calc-alkaline and alkaline types in southern and northern Da Xing'anling, respectively. Both derived from an enriched mantle [12]. Acidic volcanic rocks are divided into high Sr rhyolite and low Sr rhyolite types; high Sr rhyolite types were formed by the differentiation of calc-alkaline basaltic magma, and low Sr rhyolite types were produced by the partial melting of lower crustal rocks [13]. The interpretation of Mesozoic volcanism in this area remains controversial, with most focus placed on the mantle plume model [14–17], which is associated with the subduction of the ancient Pacific Plate [18–20] and the evolution of the Mongol-Okhotsk Ocean [18,21]. However, existing studies mainly focused on subduction,

while understanding of the Late Jurassic–Early Cretaceous tectonic evolution after the closure of the Mongol–Okhotsk Ocean remains limited [22–24]. This is of great importance for understanding the tectonic evolution of Northeast China, especially the Da Xing’anling region [25–27].

The Erguna Block is a key location for studying the characteristics of the Mongol–Okhotsk Orogenic Belt. Furthermore, Late Jurassic–Early Cretaceous magmatism was most active in the Erguna Block and its adjacent areas. Here, we investigate the zircon U–Pb ages and whole-rock geochemistry of the Late Jurassic mafic volcanic rocks in the Badaguan area of the northwestern Erguna Block. In combination with available chronological, geochemical, and isotopic data, our results provide a basis for exploring the tectonic evolution of Northeast China and its surrounding areas, and a deeper understanding of the southward subduction of the Mongol–Okhotsk Ocean.

2. Geological Setting and Sample Descriptions

Northeast China is a patchwork of miniature continental blocks, including the Erguna, Xing’an, Songnen, and Jiamusi Blocks from the northwest to the southeast (Figure 1a). The Erguna Block and the Xing’an Block were assembled before 500 Ma [28,29]. As an important component of the eastern Central Asian Orogenic Belt, the Erguna Block is located in the northern Da Xing’anling Mountains, with the Tayuan–Xiguitu Fault to the southeast, and the Mongol–Okhotsk tectonic belt to the northwest. Here, the substrate mainly consists of Neoproterozoic metamorphic volcanic-sedimentary rocks, igneous rocks, and a few Paleoproterozoic gneisses [21]. Granite, which is traditionally thought to have formed during the Mesozoic [30], is widespread throughout the Erguna Block, although recent investigations indicate that its formation occurred between the Late Triassic and the Cretaceous [19,21,24]. Along with the Late Jurassic–Early Cretaceous volcanic rocks, the granite in this region represents the largest magmatic episode in the Erguna Block [5].

Recent detailed chronological data further indicate that the Late Jurassic magmatism was more intense over the Erguna Massif. For example, the andesites found in southern Manzhouli formed during the period 156–158 Ma [13]; the basalts discovered in the Hailar Basin formed during the Late Jurassic; the basaltic andesite found in Xinlinqu formed during the period of 153–154 Ma [31]. Thus, a significant volcanic event is thought to have taken place across the entire Erguna Block during the Late Jurassic.

The detrital zircon geochronology and geochemistry of the Early Paleozoic sedimentary rocks of the Erguna Massif indicate that: (1) no uplift occurred during the Early to Middle Ordovician; (2) an uplift began during the Silurian that fed the surrounding basins; (3) the Erguna Massif was fully uplifted to the surface during the Early Devonian [32].

The study area is situated in the Badaguan area of the northwestern Erguna Block, within the Derbugan Tectonic Belt (Figure 1b). Pre-Mesozoic strata are poorly exposed in this area, with only a few metamorphic rocks of the Jiageda Formation visible near the Erguna River. Late Mesozoic volcanism was intense and widespread. From bottom to top, the volcanic rocks form an Early Jurassic–Early Cretaceous succession. Sedimentary rocks are not present in the study area. The intrusive rocks are dominated by Late Triassic syenogranite, granodiorite, and hornblende diorite [33]. The granites are closely associated with mineralization features [34,35], especially the Badaguan porphyry-type Cu–Mo polymetallic deposits. The genesis of these deposits is related to the evolution of the Mongol–Okhotsk Ocean [34,35].

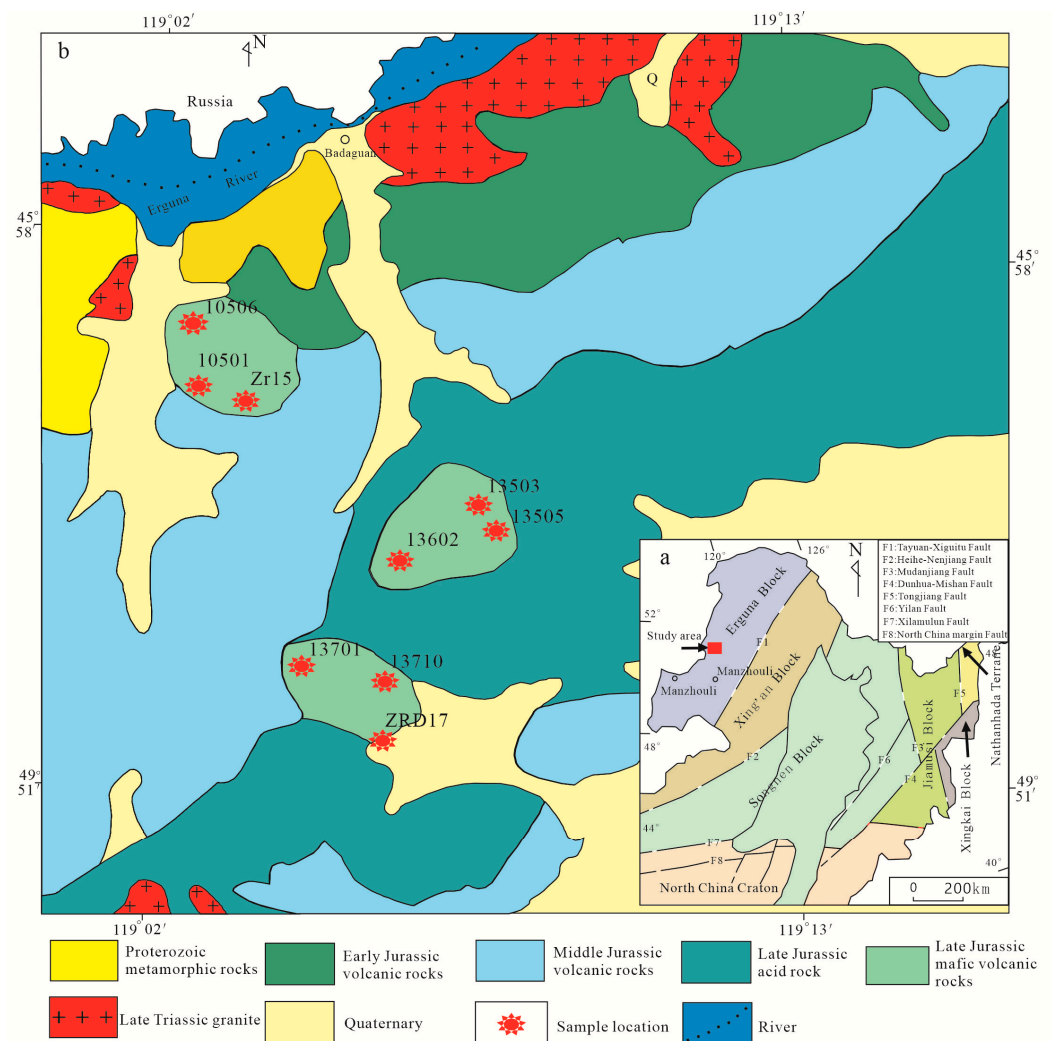


Figure 1. (a) Geological sketch map of Northeast China and (b) simplified geological map of Northwest Erguna block (modified after Li et al. [27]).

At present, there is still controversy about the opening of the Mongol-Okhotsk Ocean, but the Late Paleozoic–Mesozoic evolutionary history is relatively clear. During this period, the Mongol-Okhotsk Ocean likely subducted both northward and southward [4,34,35].

The Mongol-Okhotsk Ocean evolution can be roughly divided into seven stages: (1) during the Devonian period, the Mongol-Okhotsk oceanic crust began to subduct at a low angle beneath the Siberian plate, causing diffuse lithospheric extension and contributing to the collapse of the Early Paleozoic orogenic belt; (2) during the Early–Late Carboniferous, the subduction steepened, prompting a shift from an extensional to an extrusion regime; (3) the Late Carboniferous–Early Permian subduction plate broke off and reversed, leading to the extension of the continental lithosphere and the upwelling of mantle material; (4) Late Permian–Middle Triassic igneous rocks provide evidence for both northward and southward subduction polarity, a typical and active continental margin environment; (5) in the Late Triassic, the western part of the Mongol-Okhotsk suture zone closed, but the central and eastern oceans of the Mongol-Okhotsk Ocean were still open; (6) during the Early–Middle Jurassic period, magmatic activity in Transbaikal and North-central Mongolia weakened significantly, likely due to the subduction slowing down at its final stage, and the eventual closure of the oceans to form orogenic belts; (7) in the Late Jurassic–Early Cretaceous period, the eastern part of the Mongol-Okhotsk Ocean eventually closed, causing the granites of this period to have intraplate granite features [36–38].

The samples dated in this study were obtained from the northwestern Erguna Block. The Late Jurassic mafic volcanic rocks in the study area are exposed over an area of approximately 200 km², broadly spreading in a northeast direction, and are dominated by andesites and trachyandesites.

The andesite samples are dark in color, show a porphyritic texture, and boast a massive structure with a phenocryst content of 1–3%, with sizes ranging from 0.2 to 6 mm. The phenocrysts are dominated by plagioclase with a small amount of hornblende. The matrix comprises plagioclase microcrystals with an interwoven arrangement (Figure 2).

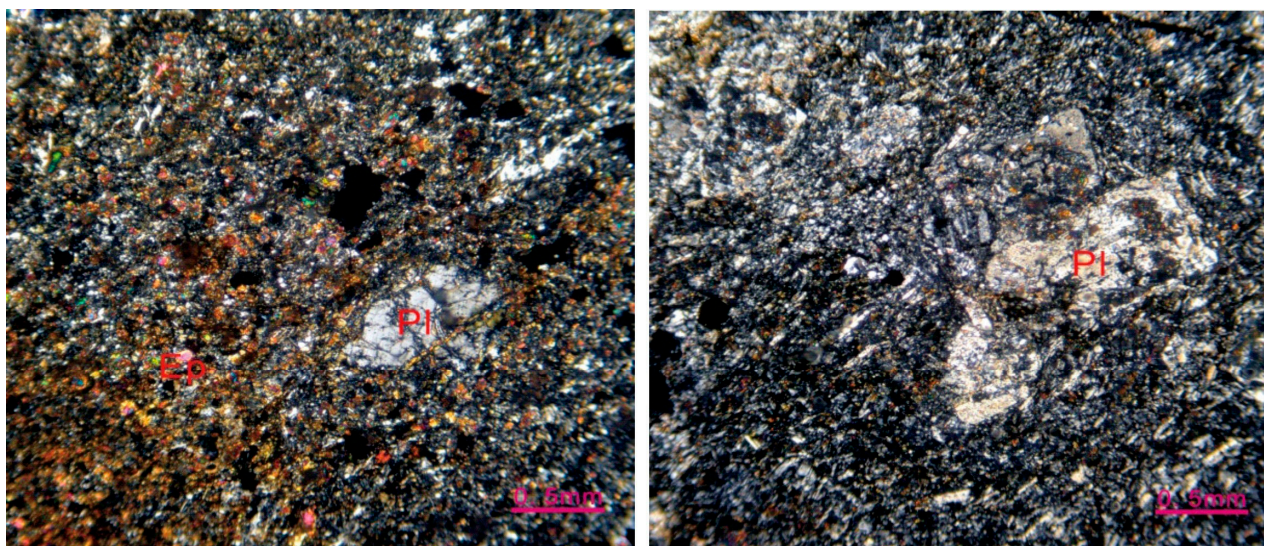


Figure 2. Micrographs of mafic volcanic rocks in the Badaguan area: Pl, plagioclase; Ep, epidote.

3. Methods

We selected nine mafic volcanic rocks for whole-rock geochemical analysis. Among them, we selected rocks with almost no alteration and moderate SiO₂ contents (samples Zr15 and ZRD17) for zircon U-Pb dating.

The whole-rock major and trace elements were analyzed at the No. 240 Institute of Nuclear Industry. The main elements were analyzed using the X-ray fluorescence (XRF) glass frit method with a relative error of <5%; trace and rare-earth elements were analyzed on an inductively coupled plasma mass spectrometer (ICP-MS) (Elan 6100DRC, Perkin Elmer, Waltham, MA, USA) alongside AVG-1 and BHVO-1 international standards, with a relative error of <5%. Zircon sorting was performed at the Langfang Regional Geological Survey Research Institute, Hebei Province, China. Zircon target making and microscopic image acquisition were conducted at the Tianjin Geological Survey Center. Laser ablation (LA) ICP-MS zircon U-Pb chronology testing was completed at the Northeast Asia Mineral Resources Evaluation Key Laboratory, Ministry of Land and Resources, Jilin University. Transmission, reflection, and cathodoluminescence images of the andesite samples were acquired to determine the type of internal zircon genesis and structural composition. For this, high-purity He gas was used as the carrier gas for the exfoliating material.

Zircon U and Pb were determined with a ComPex102 ArF excimer laser at 193 nm wavelength on an Agilent 7500a ICP-MS machine. Instrument optimization was undertaken using NIST610, a standard reference substance composed of synthetic, silicate glass developed by the American Institute of Standards and Technology. Harvard University International Standard zircon 91500 was used as an external standard. The laser beam spot diameter used for the zircon determinations was 30 µm. Analytical data were calculated using Glitter software (1999, GEMOC, Macquaric University, CSIRO, Sydney, Australia), and ordinary Pb correction was performed following [39]. For detailed experimental test procedure and instrument parameters, refer to [39].

4. Results

4.1. Zircon U-Pb Ages

Two representative andesite samples from the Late Jurassic in the Badaguan region were analyzed using zircon LA-ICP-MS dating. The measured isotope ratios and the ages calculated from the zircon single-point analysis of the two samples are listed in Table S1. Weighted mean age and concordance plots are also displayed. The zircons were well-crystallized and columnar in shape (Figure 3), with oscillating growth rings and high Th/U ratios (0.48–2.76) characteristic of their magmatic origin [40].

Sample ZRD17 (Figure 4a), an andesite, was collected in the southeast of Badaguan. A total of 20 zircons were analyzed from this sample, 13 of which were located on or near the U-Pb concordia. $^{206}\text{Pb}/^{238}\text{U}$ ages ranged from 145 to 159 Ma with a weighted average age of 157 ± 3.4 Ma, and a mean squared weighted deviation (MSWD) of 4.5. Except for seven older zircons dating from 218–377 Ma (captured age), these results indicated that the granites formed during the Late Jurassic. For sample Zr15 (Figure 4b), an andesite also collected from southeast of Badaguan, 20 zircons were analyzed, 15 of which were located on or near the U-Pb concordia. Except for five older zircons dating from 190 to 205 Ma (captured age), the $^{206}\text{Pb}/^{238}\text{U}$ ages for this sample ranged from 152 to 168 Ma with a weighted average age of 161 ± 4.4 Ma and an MSWD of 3.5.



Figure 3. Representative CL images and ages of zircons from Late Jurassic mafic volcanic rocks.

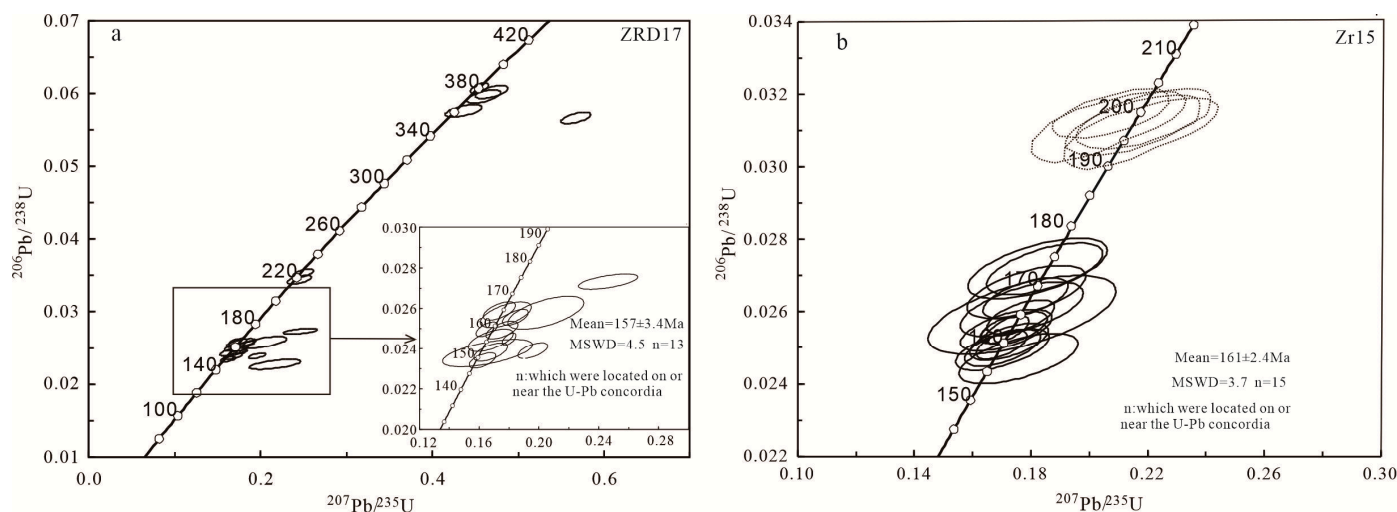


Figure 4. (a) sample ZRD17 (b) sample Zr15. Zircon U-Pb age concordia map of mafic volcanic rocks.

4.2. Whole-Rock Major and Trace Element Composition

Table S2 shows the whole-rock major trace element compositions of the nine andesite samples. These mafic volcanic rocks have SiO_2 contents of 53.55–63.68 wt %, total alkali ($\text{Na}_2\text{O} + \text{K}_2\text{O}$) contents of 4.94–9.05 wt % with CaO (1.39–4.86 wt %) and TiO_2 (0.80–1.45 wt %), high Al_2O_3 (15.49–19.86 wt %), and MgO (0.53–2.37 wt %) contents, and $\text{Mg}^\#$ values of 14.93–47.06. In the $0.001 \times \text{Zr}/\text{TiO}_2$ vs. Nb/Y diagrams, all samples except two, which are somewhat more alkaline, form one single differentiation trend and plot in the field of andesites (Figure 5).

The chondrite-normalized REE patterns indicate that all of the mafic volcanic rock samples are characterized by relatively low total REE contents ($\Sigma\text{REE} = 90.18\text{--}264.13$ ppm, average = 135.6 ppm), but are enriched in LREE, with $(\text{La}/\text{Yb})_N$ values of 8.57–17.79 and display no negative Eu anomalies (Figure 6a). The primitive-mantle-normalized trace element spider diagram (Figure 6b) further indicates that these rocks contain high Rb, Th, U, K, and LREEs, and are depleted in Nb, which is similar to subduction zone igneous rocks.

The Late Jurassic mafic volcanic rock samples from the Badaguan area show an obvious linear trend in the Harker diagram (Figure 7), suggesting that segregation and fractional crystallization may have occurred during the evolution of the magma. The negative correlation between SiO_2 and TiO_2 suggests that Fe and Ti oxides also separated and crystallized.

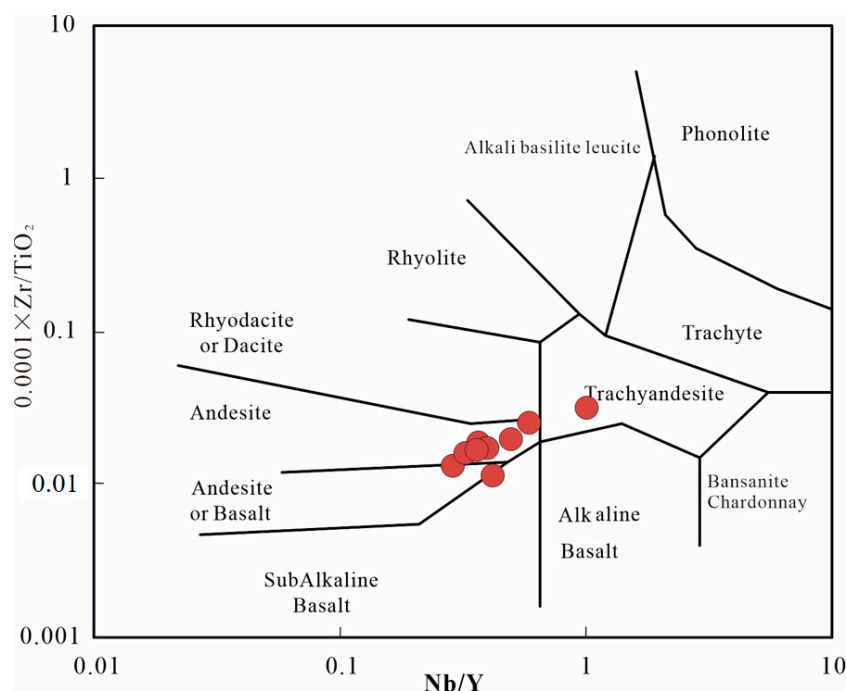


Figure 5. Plots of mafic volcanic rocks $0.0001 \times \text{Zr}/\text{TiO}_2$ versus Nb/Y diagram (modified after Winchester et al. [41]).

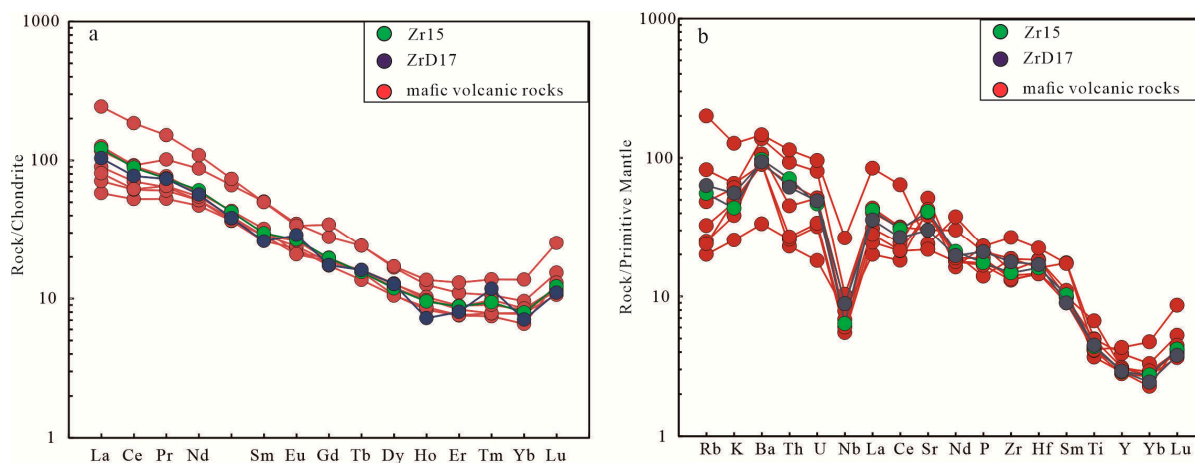


Figure 6. Chondrite-normalized REE patterns (a) and primitive-mantle-normalized trace element spider diagrams (b) for the Late Jurassic mafic volcanic rocks in Badaguan area (modified after Sun et al. [42]).

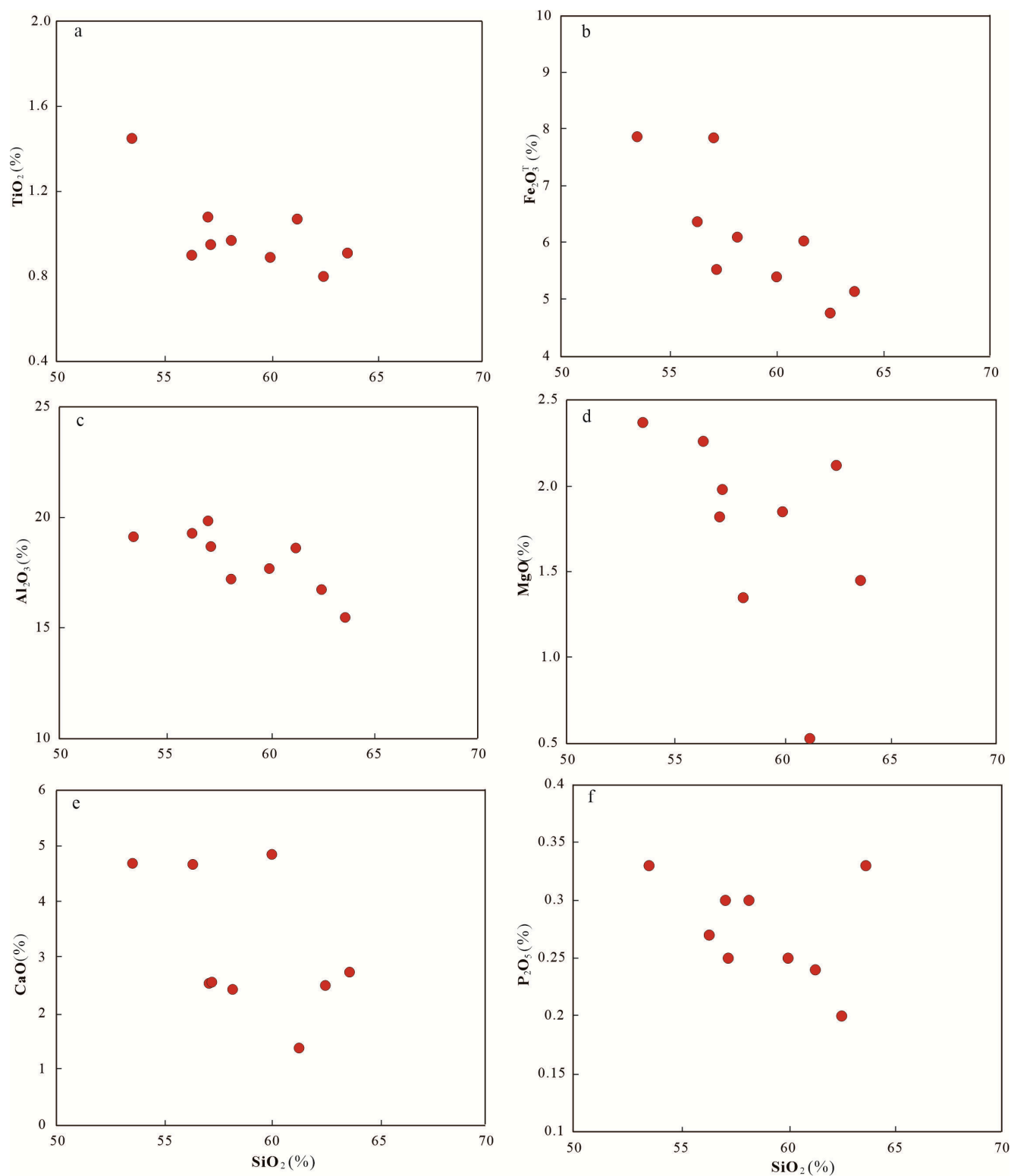


Figure 7. Harker diagram of Late Jurassic mafic volcanic rocks from Badaguan area. (a) TiO₂ vs. SiO₂ diagram; (b) Fe₂O₃ vs. SiO₂ diagram; (c) Al₂O₃ vs. SiO₂ diagram; (d) MgO vs. SiO₂ diagram; (e) CaO vs. SiO₂ diagram; (f) P₂O₅ vs. SiO₂ diagram.

5. Discussion

5.1. Ages of Mafic Volcanic Rocks

Due to the lack of accurate age and biostratigraphic information, the age of the volcanic-bearing strata in the Da Xing'anling area was mainly determined based on rock assemblage features and regional stratigraphic correlations. The Late Jurassic mafic volcanic rocks in the Badaguan area are similar to those of the Tamurangou Formation, which lack isotopic age data. Some researchers consider these rocks as belonging to the Middle Jurassic Tamurangou Formation [30]. However, our new U-Pb zircon data indicate otherwise. Our derived ages (157–161 Ma) correspond to the Late Jurassic, which is younger than the previously assumed Middle Jurassic age of these rocks.

5.2. Petrogenesis and the Nature of the Magma Source

Calc-alkaline, or transitional mafic volcanic, rocks are an essential part of orogenic belts, and understanding their genesis is of great importance for revealing the formation, growth, and crust–mantle interaction of the Earth's crust [43]. Based on previous research, the following processes have been proposed regarding the genesis of calc-alkaline or transitional mafic volcanic rocks: (1) partial melting of the lithospheric mantle, metasomatized by subduction-related fluids [4,24,44,45]; (2) separation and crystallization of mantle-derived basaltic magma [46]; (3) mixing of crust-sourced feldspathic magma with mantle-sourced basaltic magma [47]; and (4) the partial melting of subcrustal material due to the intrusion of mantle-derived basaltic magma at the base [48,49].

The studied mafic volcanic rocks are relatively low in SiO₂ content (53.55–63.68 wt %), but high in Al₂O₃ (15.49–19.86 wt %) and MgO (0.53–2.37 wt %), and have Mg[#] values of 14.93–47.06. Furthermore, the crustal source magma has relatively high Lu/Yb (0.16–0.18) and Rb/Sr (>0.5) ratios. In contrast, the Lu/Yb and Rb/Sr ratios of the Late Jurassic mafic volcanic rock samples in the study area range from 0.20 to 0.29 and from 0.01 to 0.08, respectively, which are significantly lower than those of crustal-sourced magmas. Indeed, the Lu/Yb (0.14–0.15) and Rb/Sr (0.03–0.047) ratios are similar to those of mantle-derived magma [50]. Therefore, our results indicate that the Late Jurassic mafic volcanic rocks in the Badaguan area were not the product of the partial melting of the mafic lower crust.

In addition, the Late Jurassic volcanic rocks in the northern Da Xing'anling region are dominated by andesites and rhyolites, with some inclusions, but contain no large-scale basaltic magmatic rocks [5]. The characteristics of mafic volcanic rocks in the Badaguan area imply that they are not the product of the differentiation of basaltic magma. The zircon Lu-Hf isotopic system has a high confinement temperature, and when magma mixing occurs, previously crystallized zircon can effectively record the Hf isotopic signature of the mixed end elements [4]. Both Lu and Hf are incompatible trace elements and relatively immobile; however, Hf is more incompatible than Lu and is relatively enriched in the crust and in silicate melts. U-Pb and Lu-Hf isotope systems in zircon record crust–mantle differentiation through time, i.e., fluid-assisted melt extraction from the mantle to form juvenile crust. Negative ϵ_{Hf} values reflect enrichment with respect to the bulk Earth, while positive ϵ_{Hf} values (0 to +15) reflect an origin from a source intermediate between depleted mantle (DM) and bulk Earth. Therefore, when the value of $\epsilon_{\text{Hf}}(t)$ is negative, it usually represents the remelting of ancient crust or the mixing of ancient crust during the formation of magma. When the value of $\epsilon_{\text{Hf}}(t)$ is both positive and negative, it may mean that the granite is of mixed crust–mantle origin. With positive $\epsilon_{\text{Hf}}(t)$ values, the magma is derived from the partial melting of new basal crustal material added from the depleted mantle [4,5].

Previously published data from the Erguna Block have also shown that the zircons have a relatively homogeneous Hf isotopic composition (Figure 8). From these data, it seems that there is a rough evolution through time toward more depleted mantle sources, with $\epsilon_{\text{Hf}}(t)$ values ranging between +0.7 and +11.0, and the corresponding second-stage model (TDM₂) ages ranging from 441 to 1156 Ma (Table S3 [51–55]). This implies that magma mixing was not the main pathway of the mafic magma [5]. Slab melts and lower

crust melts can also react with the mantle to form mafic magmas, which are characterized by adakites with high Sr/Y ratios and low Y and Yb contents. The mafic volcanic rocks from the Badaguan area have relatively low Sr/Y ratios and high Y and Yb contents (Figure 9a), which differs from the adakites of subduction slab or subcrustal detachment but is similar to typical arc volcanic rocks. These rocks are distinctly different from the magmas produced by the partial melting of basal lower crustal material [49].

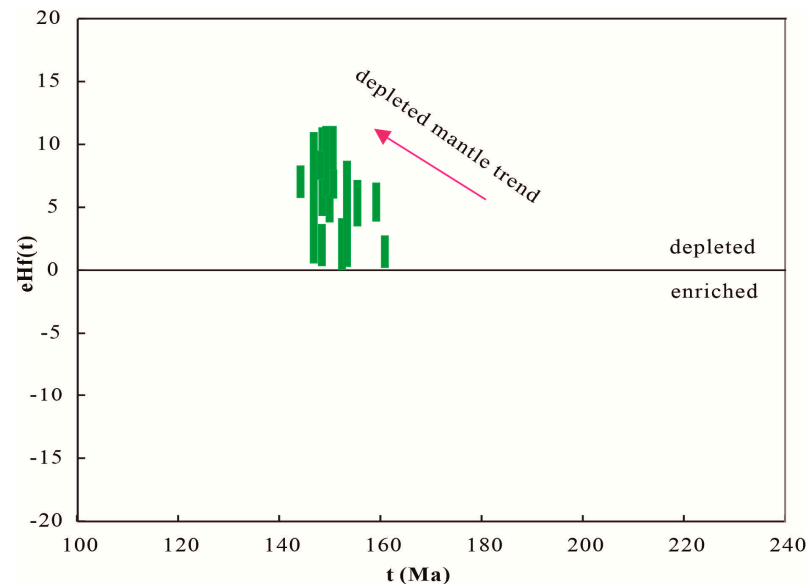


Figure 8. Plots of zircon Hf isotopic compositions versus ages of Late Jurassic igneous rocks in the Erguna Massif. Data sources are listed in Table S3.

Mantle-derived magma in the process of upward intrusion would have inevitably experience crustal material mixing. Small amounts of captured zircon suggest that crustal material mixing may have occurred.

Although some of the mafic volcanic rocks have high K_2O/P_2O_5 ratios, and the K_2O/P_2O_5 ratios are positively correlated with their SiO_2 content, the K_2O/P_2O_5 ratios of most of the samples show little variation, and do not increase with increasing SiO_2 content (Figure 9b). Combined with the references in Table S3 for the Erguna Block [51–55], these observations imply that the mafic magma in this region did not undergo significant crustal contamination during its ascent through the continental crust.

Nb/La-Ba/Rb diagrams can distinguish between crustal mixing and a single mantle source. The evolution of mantle-derived magma via crustal mixing results in a wide range of Nb/La values and a narrow range of Ba/Rb values; in contrast, the Ba/Rb values of enriched mantle are variable, and Nb/La values are highly consistent [56–58]. The studied mafic volcanic rocks show a parallel trend in the Nb/La-Ba/Rb diagram (Figure 9c), indicating that the magma is not mixed with crustal material. Furthermore, the geochemical characteristics mainly reflect the magma source area. However, mafic magma mixed with crustal material has high $^{87}Sr/^{86}Sr$ ratios positively correlated with SiO_2 content, whereas the $^{87}Sr/^{86}Sr$ ratios of the mafic volcanic rocks in the Manzhouli area of the Erguna Massif show a low degree of variation, and do not increase with increasing SiO_2 content [58]. Thus, the degree of crustal material contamination in the study region is likely low.

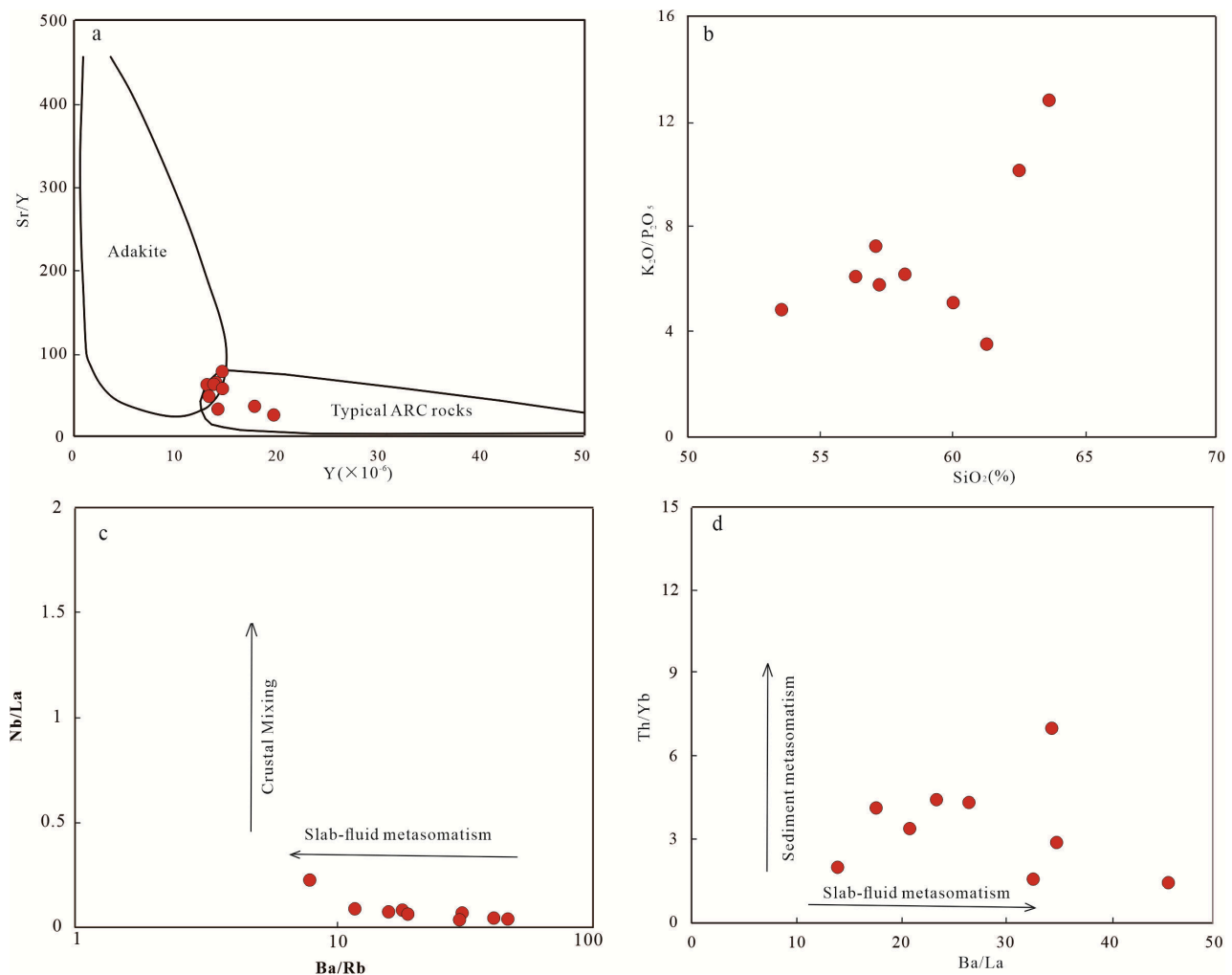


Figure 9. (a) Sr/Y vs. Y diagram (modified after Defant and Drummond [59]). (b) K_2O/P_2O_5 vs. SiO_2 diagram (modified after Ji et al. [4]). (c) Nb/La vs. Ba/Rb diagram. (d) Th/Yb vs. Ba/La diagram (modified Woodhead et al. [56]) for mafic volcanic in Badaguan area.

The main mechanism of lithospheric mantle enrichment is subduction metasomatism, involving fluids formed by dewatering of the oceanic crust, and melt accounting for oceanic sediments. The influence of subduction-related fluids and sediment melt can be determined based on trace element ratios. Fluid-mobile elements (e.g., Ba, Rb, and Sr) are easily transported in aqueous fluids, while melt-active elements (e.g., Th and La) easily enter the sediment melt. Accordingly, the ratio of fluid, sedimentary melt activity elements, and weakly active HFSEs or heavy rare-earth elements (HRESs) indicates the contribution of subduction fluids and sediment melts to the source region. The Late Jurassic mafic volcanic rocks from the study region generally correspond to subduction-related fluid, while individual samples have high Th/Yb ratios (Figure 9d) indicating the possible addition of subducting sediments. Taken together, these results indicate that the Late Jurassic mafic volcanic rocks in the Badaguan region are derived from the partial melting of the lithosphere, metasomatized by subduction-related fluid, with the possible addition of subducting sediments.

5.3. Tectonic Background of Andesite Formation

Late Jurassic volcanic rocks are mainly distributed in the Da Xing'anling Mountains on the south side of the Mongol-Okhotsk suture zone; volcanism was largely absent during this period in the Songliao Basin and eastern Jihei [4,60,61]. As the subduction direction of

the ancient Pacific Plate relative to Eurasia was northward during this period, the spatial and temporal distribution of the volcanic rocks suggests that their formation was mainly related to the evolution of the Mongol-Okhotsk Ocean. In recent years, the detailed study of the Early Mesozoic granites and porphyry copper-molybdenum deposits in the Manzhouli-Erguna area [62,63] has confirmed the southward subduction of the Mongol-Okhotsk Ocean. The formation of the Late Triassic Taipingshan and Badaguan porphyry copper-molybdenum ores and the Early Jurassic Unugtushan porphyry copper-molybdenum ores reflects the tectonic background of the active continental margin during this period. Furthermore, the coeval granites are mainly granodiorite diorite granite assemblages, which are similar to those forming at active continental margins, supporting the southward subduction of the Mongol-Okhotsk Ocean.

Based on our analyses of the Mesozoic igneous rocks of the Erguna Massif, the calc-alkaline or transitional igneous rock assemblages are Early–Late Jurassic in age. The development of bimodal volcanic rocks in the Early Cretaceous and the change in magmatism characteristics record the transition from the Early Jurassic oceanic subduction to the Late Jurassic post-orogenic extension of the Mongol-Okhotsk Ocean [2,64]. Most of the Late Mesozoic igneous rocks of the Erguna Massif are of type A and A₂ [64], formed by lithospheric extension after the closure of the Mongol–Okhotsk Ocean. At the same time, the igneous rocks from this period tend to change from adakites to calc-alkaline igneous rocks, indicating that the granite source rocks formed by partial melting during the extensional collapse and crustal thinning of the Mongol-Okhotsk Orogenic Belt [65,66].

The Late Jurassic mafic volcanic rocks in the Badaguan area of the northern section of the Da Xing'anling region have typical geochemical characteristics of subduction-related fluid, which are enriched in large ionic lithophile elements (e.g., Rb, Th, U, and K) and depleted in HFSEs and HREEs. These rocks also have high Nb contents. Our samples are plotted in the continental arc region of the Th/Yb–Nb/Yb diagram (Figure 10a), suggesting that they formed in an active continental margin environment. Indeed, the samples have high La/Yb and Th/Yb ratios similar to Andean-type active continental margin andesites (Figure 10b). All studied rocks plotted within the field of subduction-related IAB series, forming a mixing trend toward more depleted mantle sources (Figure 10c).

The Late Jurassic mafic volcanic rocks in the Badaguan area may be derived from the partial melting of the lithosphere, metasomatized by subduction-related fluid, with the possible addition of subducting sediments. This tectonic background is closely related to the evolution of the Mongol–Okhotsk Ocean. This interpretation is consistent with the tectonic context displayed by the bimodal volcanic rocks at Tamurangou (160–164 Ma) and Manketourbo (159–162 Ma), as well as the A1 rhyolite of the Baiyingaolao Formation (139–142 Ma) [12,13,50]. This is broadly consistent with the timing of the formation of mafic volcanic rocks in the study region. Finally, the northwest part of the Erguna Massif is very close to the Mongol-Okhotsk suture zone; the Middle–Late Jurassic volcanic rocks only occur in the western part of the Songliao Basin, and tend to be younger and deeper in the source area from west to east [13]. These rocks likely derived from the partial melting of the lithosphere, previously metasomatized by subduction-related fluid, with some contribution of subducted sediments; these sediments belonged to a Late Jurassic–Early Cretaceous suite of magmatic rocks that evolved from a typical calc-alkaline “active margin” type toward a more depleted or, alternatively, more alkaline type during post-collisional crust delamination.

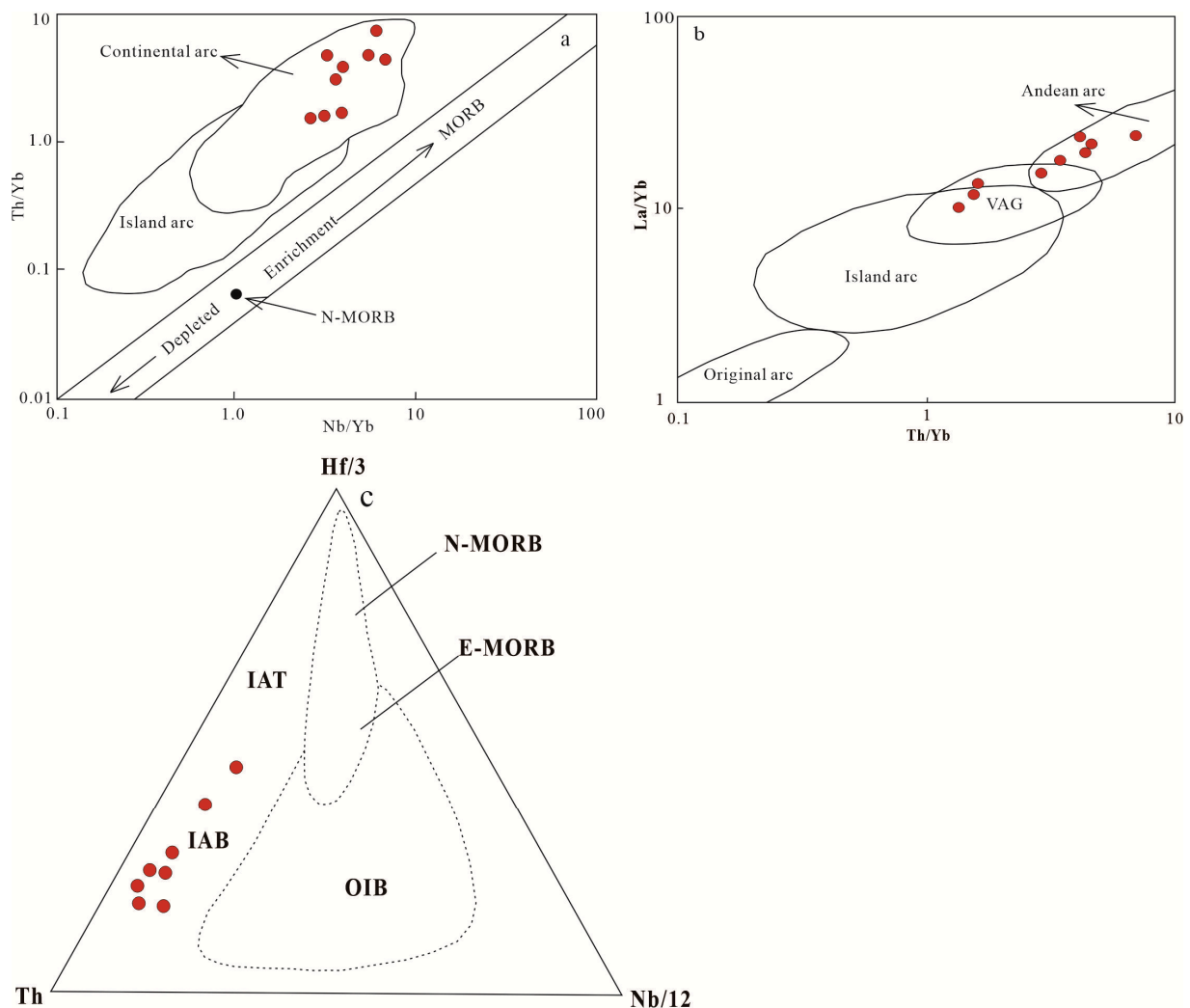


Figure 10. (a) Th/Yb vs. Nb/Yb diagram (modified after Li et al. [67]). (b) La/Yb vs. Th/Yb diagram (modified after Bailey [68]) mafic volcanic in Badaguan area. (c) Classical discriminant diagram Hf/3-Th-Nb/12 (modified after Wood [69]). MORB: mid ocean ridge basalt.

6. Conclusions

Based on the chronology and geochemistry of the mafic volcanic rocks in the Badaguan area combined with existing research, we draw the following main conclusions:

- (1) The mafic volcanic rocks of the Badaguan area in the northern part of the Da Xing'anling Mountains region formed during the Late Jurassic (157–161 Ma).
- (2) These rocks likely derived from the partial melting of the lithosphere, previously metasomatized by subduction-related fluid with some contribution of subducted sediments.
- (3) The studied mafic volcanic rocks likely formed by lithospheric extension after the closure of the Mongol-Okhotsk Ocean.

Supplementary Materials: The following are available online at <https://www.mdpi.com/article/10.3390/min11091010/s1>, Table S1: Zircon U–Pb isotopic data for the Badaguan andesite in the Erguna Block. Table S2: Major (wt %) and trace element (ppm) data for mafic volcanic rocks in the Erguna Block. Table S3: Age and Hf isotopic data of Late Jurassic igneous rocks in the Erguna Massif.

Author Contributions: Y.L., Z.-B.Y. and F.-J.N., designed the project; Y.L. wrote and organized the paper, with a careful discussion and revision by Z.-B.Y., and F.-J.N. All authors have read and agreed to the published version of the manuscript.

Funding: This work was financially supported by China Geological Survey (grant No. 12120113053700) and Fundamental Science on Radioactive Geology and Exploration Technology Laboratory, East China University of Technology (grant No. 2020RGET02).

Data Availability Statement: The data presented in this study are available in this article.

Acknowledgments: We thank Zhibin Han, Xiaoguang Hou from the No. 240 Institute of Nuclear Industry for their kind help with the analysis of the zircon ages.

Conflicts of Interest: The authors declare no conflict of interest.

References

1. Zhang, J.H.; Gao, S.; Ge, W.C.; Wu, F.Y.; Yang, J.H.; Wilde, S.A.; Li, M. Geochronology of the Mesozoic volcanic rocks in the Great Xingan Range, northeastern China: Implications for subduction induced delamination. *Chem. Geol.* **2010**, *276*, 144–165. [[CrossRef](#)]
2. Xu, W.L.; Pei, F.P.; Wang, F.; Meng, E.; Ji, W.Q.; Yang, D.B.; Wang, W. Spatial-temporal relationships of Mesozoic volcanic rocks in NE China: Constrain on tectonic overprinting and transformations between multiple tectonic regimes. *J. Asian Earth Sci.* **2013**, *74*, 167–193. [[CrossRef](#)]
3. Liu, Y.J.; Li, W.M.; Feng, Z.Q.; Wen, Q.B.; Neubauer, F.; Liang, C.Y. Review of the Paleozoic tectonics in the eastern part of Central Asian Orogenic Belt. *Gondwana Res.* **2017**, *43*, 123–148. [[CrossRef](#)]
4. Ji, Z.; Ge, W.C.; Yang, H.; Bi, J.H.; Yu, Q.; Dong, Y. The late Triassic Andean type andesite from the central Great Xingan Range: Produces of the southward subduction of the Mongol Okhotsk oceanic plate. *Acta Petrol. Sin.* **2018**, *34*, 2917–2930. (In Chinese with English Abstract)
5. Mao, A.Q.; Sun, D.Y.; Yang, D.G.; Tang, Z.Y.; Zheng, H. Petrogenesis and tectonic implications of Early Cretaceous volcanic rocks from the Shanghulin Basin within the north-western Great Xing’an Range, NE China: Constraints from geochronology and geochemistry. *Geol. J.* **2019**, *55*, 3476–3496. [[CrossRef](#)]
6. Jin, R.S.; Miao, P.S.; SiMa, X.Z.; Li, J.G.; Zhao, H.L.; Zhao, F.Q.; Feng, X.X.; Chen, Y.; Chen, L.L.; Zhao, L.J. Structure styles of Mesozoic-Cenozoic U-bearing rock series in Northern China. *Acta Geol. Sin.* **2016**, *90*, 2104–2116. [[CrossRef](#)]
7. Wang, F.F.; Liu, C.Y.; Qiu, X.W.; Guo, P.; Zhang, S.H.; Cheng, X.H. Characteristics and distribution of world’s identified sandstone-type uranium resources. *Acta Geol. Sin.* **2017**, *91*, 2021–2046. (In Chinese with English Abstract)
8. Wang, W. Geochronology and Geochemistry of the Early Jurassic Volcanic Rocks in the Manzhouli-Erguna Area, NE China, Inner Mongolia. Master’s Thesis, Jilin University, Changchun, China, 2014; pp. 1–100. (In Chinese with English Abstract)
9. Zhou, J.B.; Wilde, S.A.; Zhao, G.C.; Han, J. Nature and assembly of microcontinental blocks within the Paleo-Asian Ocean. *Earth Sci. Rev.* **2018**, *186*, 76–93. [[CrossRef](#)]
10. Zhang, J.H.; Ge, W.C.; Wu, F.Y.; Wilde, S.A.; Yang, J.H.; Liu, X.M. Large-scale Early Cretaceous volcanic events in the northern Great Xing’an Range, northeastern China. *Lithos* **2008**, *102*, 138–157. [[CrossRef](#)]
11. Cheng, Y.H.; Li, Y.; Wang, S.Y.; Li, Y.F.; Ao, C.; Li, J.G.; Sun, L.X.; Li, H.L.; Zhang, T.F. Late Cretaceous tectono-magmatic event in Songliao Basin, NE China: New insights from mafic dyke geochronology and geochemistry analysis. *Geol. J.* **2018**, *53*, 2991–3008. [[CrossRef](#)]
12. Ge, W.C.; Lin, Q.; Sun, D.Y.; Wu, F.Y.; Li, X.H. Geochemical research into origins of two types of mesozoic rhyolites in Daxing’anling. *Earth Sci.* **2000**, *25*, 172–178. (In Chinese with English Abstract)
13. Zhao, Z.H.; Sun, D.Y.; Gou, J.; Ren, Y.S.; Fu, C.L.; Zhang, X.Y.; Wang, X.; Liu, X.M. Chronology and geochemistry of volcanic rocks in Tamulangou Formation from Southern Manzhouli, Inner—Mongolia. *J. Jilin Univ. (Earth Sci. Ed.)* **2011**, *41*, 1865–1879. (In Chinese with English Abstract)
14. Lin, Q.; Ge, W.C.; Sun, D.Y.; Wu, F.Y. Geomechanical significance of the Mesozoic volcanics in Northeast Asia. *Chin. J. Geophys.* **1999**, *42*, 75–84. (In Chinese with English Abstract)
15. Lin, Q.; Ge, W.C.; Sun, D.Y.; Wu, F.Y.; Chong, K.W.; Kyung, D.M.; Myung, S.J.; Moon, W.W.; Chi, S.K.; Sung, H.Y. Tectonic significance of Mesozoic volcanic rocks in Northeastern China. *Sci. Geol. Sin.* **1998**, *33*, 129–139. (In Chinese with English Abstract)
16. Deng, J.F.; Mo, X.X.; Zhao, H.L.; Wu, Z.X.; Luo, Z.H.; Su, S.G. A new model for the dynamic evolution of Chinese lithosphere: Continental roots-plume tectonics. *Earth Sci. Rev.* **2004**, *65*, 223–275. [[CrossRef](#)]
17. Lin, Q.; Ge, W.C.; Cao, L.; Sun, D.Y.; Lin, J.G. Geochemistry of Mesozoic volcanic rocks in Daxing’anling: The bimodal volcanic rocks. *Geochimica* **2003**, *32*, 208–222. (In Chinese with English Abstract)
18. Wang, P.J.; Chen, F.K.; Shen, S.M. Geochemical and Nd-Sr-Pb isotopic composition of Mesozoic volcanic rocks in the Songliao basin, NE China. *Geochem. J.* **2006**, *40*, 149–159. [[CrossRef](#)]
19. Zhang, J.H.; Ge, W.C.; Wu, F.Y.; Liu, X.M. Mesozoic bimodal volcanic suite in Zhalantun of the Da Hinggan Range and its geological significance: Zircon U-Pb age and Hf isotopic constraints. *Acta Geol. Sin.* **2006**, *80*, 58–69.
20. Chen, L.L.; Cheng, Z.G. Petrology and zircon chronology of the Dorolj in Hinggan League, Inner Mongolia. *Geol. China* **2015**, *42*, 891–908. (In Chinese with English Abstract)

21. Zhang, L.C.; Chen, Z.G.; Zhou, X.H.; Ying, J.F.; Zhang, Y.T. Characteristics of deep sources and tectonic-magmatic evolution of the early Cretaceous volcanics in Genhe area. Da-Hinggan Mountains: Constraints of Sr-Nd-Pb-Hf isotopic geochemistry. *Act. Petrol. Sinic.* **2007**, *23*, 2823–2835, (In Chinese with English abstract).
22. Li, J.Y. Permian geodynamic setting of Northeast China and adjacent regions: Closure of the Paleo Asian Ocean and subduction of the Paleo Pacific Plate. *J. Asian Earth Sci.* **2006**, *26*, 207–224. [[CrossRef](#)]
23. Wang, W.; Tang, J.; Xu, W.L.; Wang, F. Geochronology and geochemistry of Early Jurassic volcanic rocks in the Erguna Massif, northeast China: Petrogenesis and implications for the tectonic evolution of the Mongol–Okhotsk suture belt. *Lithos* **2015**, *218–219*, 73–86. [[CrossRef](#)]
24. Dong, Y.; Ge, W.C.; Yang, H.; Wang, Q.; Zhang, Y.; Su, L. Geochronology and geochemistry of Early Cretaceous volcanic rocks from the Baiyingaolao Formation in the central Great Xing’an Range, NE China, and its tectonic implications. *Lithos* **2016**, *205*, 168–184. [[CrossRef](#)]
25. Tang, J.; Xu, W.L.; Wang, F.; Wang, W.; Xu, M.J.; Zhang, Y.H. Geochronology and geochemistry of Neoproterozoic magmatism in the Erguna Massif, NE China: Petrogenesis and implications for the breakup of the Rodinia supercontinent. *Precambrian Res.* **2013**, *224*, 597–611. [[CrossRef](#)]
26. Mi, K.; Liu, Z.; Li, C.; Liu, R.; Wang, J.; Peng, R. Origin of the Badaguan porphyry Cu-Mo deposit, Inner Mongolia, northeast China: Constraints from geology, isotope geochemistry and geochronology. *Ore Geol. Rev.* **2017**, *81*, 154–172. [[CrossRef](#)]
27. Li, Y.; Wang, J.; Han, Z.; Hou, X.G.; Wang, S.Y. Zircon U-Pb dating and petrogenesis of the early Jurassic Rhyolite in Badaguan from Northern of Daxinganling Mountains. *Geol. China* **2017**, *47*, 346–357. (In Chinese with English Abstract)
28. Liu, H.C.; Li, Y.L.; He, H.Y.; Huangfu, P.P.; Liu, Y.Z. Two-phase southward subduction of the Mongol-Okhotsk oceanic plate constrained by Permian-Jurassic granitoids in the Erguna and Xing’an massifs (NE China). *Lithos* **2018**, *304–307*, 347–361. [[CrossRef](#)]
29. Ge, W.C.; Wu, F.Y.; Zhou, C.Y.; Abdel Rahman, A.A. Emplacement age of the Tahe granite and its constraints on the tectonic nature of the Erguna block in the northern part of the Da Xing’an Range. *Chin. Sci. Bull.* **2005**, *50*, 2097–2105. [[CrossRef](#)]
30. IMBGMR (Inner Mongolia Bureau of Geology Mineral Resources). *Stratigraphy (Lithostratigraphic) of Nei Mongol Autonomous Region*; China University of Geosciences Press: Wuhan, China, 1996; p. 344. (In Chinese with English Abstract)
31. Yang, Y.T.; Guo, Z.X.; Song, C.C.; Li, X.B.; He, S. A short-lived but significant Mongol-Okhotsk collisional orogeny in latest Jurassic-earliest Cretaceous. *Gondwana Res.* **2015**, *28*, 1096–1116. [[CrossRef](#)]
32. Lin, T.; Ji, F.; Bian, H.Y.; Sun, K.; Zhang, S.J.; Biao, S.H. Exhumation time of basement-uplift constrained by ages of the detrital zircons from Paleozoic clastic rocks in Fulin area, Great Hinggan Mountains. *Geol. Rev.* **2015**, *61*, 402–414.
33. Miao, L.C.; Liu, D.Y.; Zhang, F.Q.; Fan, W.M.; Shi, Y.R.; Xie, H.Q. Zircon SHRIMP U–Pb ages of the “Xinghuadukou Group” in Hanjiayuanzi and Xinlin areas and the “Zhalantun Group” in Inner Mongolia, Da Hinggan mountains. *Chin. Sci. Bull.* **2007**, *52*, 1112–1134. [[CrossRef](#)]
34. Deng, C.Z.; Li, G.H. The Cu-Mo mineralization of the Late Jurassic porphyry in the Northern Great Xing’an Range: Constraints from zircon U-Pb ages of the Ore-Causative Granites. *Acta Geol.* **2019**, *93*, 236–237. [[CrossRef](#)]
35. Gou, J.; Sun, D.Y.; Ren, Y.S.; Liu, Y.J.; Zhang, S.Y.; Fu, C.L.; Liu, X.M. Petrogenesis and geodynamic setting of Neoproterozoic and Late Paleozoic magmatism in the Manzhouli-Erguna area of Inner Mongolia, China: Geochronological, geochemical and Hf isotopic evidence. *J. Asian Earth Sci.* **2013**, *67–68*, 114–137. [[CrossRef](#)]
36. Donskaya, T.V.; Gladkochub, D.P.; Mazukabzov, A.M. Late Paleozoic-Mesozoic subduction-related magmatism at the southern margin of the Siberian continent and the 150 million-year history of the Mongol-Okhotsk Ocean. *J. Asian Earth Sci.* **2013**, *62*, 79–97. [[CrossRef](#)]
37. Sorokin, A.A.; Kudryashov, N.M.; Li, J.Y.; Zhuravlev, D.Z.; Yan, P.; Sun, G.H.; Gao, L.M. Early Paleozoic granitoids in the eastern margin of the Argun terrane, Amur area: First geochemical and geochronologic data. *Petrology* **2004**, *12*, 367–376.
38. Sorokin, A.A.; Zaiika, V.A.; Kovach, V.P.; Kotov, A.B.; Xu, W.; Yang, H. Timing of closure of the eastern Mongol-Okhotsk Ocean: Constraints from U-Pb and Hf isotopic data of detrital zircons from metasediments along the Dzhagdy Transect. *Gondwana Res.* **2020**, *81*, 58–78. [[CrossRef](#)]
39. Anderson, T. Correction of common lead in U-Pb analyses that do not report ^{204}Pb . *Chem. Geol.* **2002**, *192*, 59–79. [[CrossRef](#)]
40. Belousova, E.A.; Griffin, W.L.; O’Reilly, S.Y. Igneous zircon: Trace element composition as an indicator of source rock type. *Contrib. Mineral. Petrol.* **2002**, *143*, 602–622. [[CrossRef](#)]
41. Maniar, P.D.; Piccoli, P.M. Tectonic discrimination of granitoids. *Geol. Soc. Am. Bull.* **1989**, *101*, 635–643. [[CrossRef](#)]
42. Sun, S.S.; McDonough, W.F. Chemical and Isotopic Systematics of Oceanic Basalts: Implications for Mantle Composition and Processes. In *Magmatism in Ocean Basins*; Saunders, A.D., Norry, M.J., Eds.; Geological Society of Special Publication: London, UK, 1989; Volume 27, pp. 313–345.
43. Chen, L.; Zhao, Z.F. Origin of continental arc andesites: The composition of source rocks is the key. *J. Asian Earth Sci.* **2017**, *145*, 217–232. [[CrossRef](#)]
44. Yu, Q.; Ge, W.C.; Zhang, J.; Zhao, G.C.; Zhang, Y.L.; Yang, H. Geochronology, petrogenesis and tectonic implication of Late Paleozoic volcanic rocks from the Dashizhai Formation in Inner Mongolia, NE China. *Gondwana Res.* **2017**, *43*, 164–177. [[CrossRef](#)]
45. Zheng, H.; Sun, X.M.; Wan, K.; Wang, P.J.; He, S.; Zhang, X.Q. Structure and tectonic evolution of the Late Jurassic–Early Cretaceous Wandashan accretionary complex, NE China. *Int. Geol. Rev.* **2019**, *61*, 17–38. [[CrossRef](#)]

46. Lee, C.T.A.; Lee, T.C.; Wu, C.T. Modeling the compositional evolution of recharging, evacuating, and fractionating (REFC) magmas Chambers: Implications for differentiation of arc magmas. *Geochim. Cosmochim. Acta* **2014**, *143*, 8–22. [[CrossRef](#)]
47. Guo, F.; Nakamura, E.; Fan, W.M.; Kobayashi, K.; Li, C.W. Generation of Palaeocene adakitic andesites by magma mixing in Yanji area, NE China. *J. Petrol.* **2007**, *48*, 661–692. [[CrossRef](#)]
48. Jung, S.; Hoernes, S.; Mezger, K. Synorogenic melting of mafic lower crust: Constraints from geochronology, petrology and Sr, Nd, Pb and O isotope geochemistry of quartz diorites (Damara orogen, Namibia). *Contrib. Mineral. Petrol.* **2002**, *143*, 551–566. [[CrossRef](#)]
49. Rapp, R.P.; Watson, E.B. Dehydration melting of metabasalt at 8–32 kbar: Implications for continental growth and crust mantle recycling. *J. Petrol.* **1995**, *36*, 891–931. [[CrossRef](#)]
50. Sun, D.Y.; Gou, J.; Ren, Y.S.; Fu, C.L.; Wang, X.; Liu, X.M. Zircon U–Pb dating and study on geochemistry of volcanic rocks in Manitu Formation from southern Manchuria, Inner Mongolia. *Acta Petrol. Sin.* **2011**, *27*, 3083–3094. (In Chinese with English Abstract)
51. Sun, D.Y.; Gou, J.; Wang, T.H.; Ren, Y.S.; Liu, Y.J.; Guo, H.Y.; Zhao, C.H. Geochronological and geochemical constraints on the Erguna massif basement, NE China—Subduction history of the Mongol–Okhotsk oceanic crust. *Int. Geol. Rev.* **2013**, *55*, 1801–1816. [[CrossRef](#)]
52. Wang, T.H.; Zhang, S.Y.; Sun, D.Y.; Gou, J.; Ren, Y.S.; Wu, P.F.; Liu, X.M. Zircon U–Pb ages and Hf isotopic characteristics of Mesozoic granitoids from southern Manzhouli, Inner Mongolia. *Glob. Geol.* **2014**, *33*, 26–33. (In Chinese with English Abstract)
53. Tang, J.; Xu, W.L.; Wang, F.; Zhao, S.; Li, Y. Geochronology, geochemistry, and deformation history of Late Jurassic–Early Cretaceous intrusive rocks in the Erguna Massif, NE China: Constraints on the late Mesozoic tectonic evolution of the Mongol–Okhotsk Orogenic belt. *Tectonophysics* **2015**, *658*, 91–110. [[CrossRef](#)]
54. Shi, L.; Zheng, C.Q.; Yao, W.G.; Li, J.; Cui, F.; Gao, F.H.; Han, X.M. Geochronological framework and tectonic setting of the granitic magmatism in the Chaihe–Moguqi region, central Great Xing’an Range, China. *J. Asian Earth Sci.* **2015**, *113*, 443–453. [[CrossRef](#)]
55. Gou, J.; Sun, D.Y.; Liu, Y.J.; Ren, Y.S.; Zhao, Z.H.; Liu, X.M. Geochronology, petrogenesis, and tectonic setting of Mesozoic volcanic rocks, southern Manzhouli area, Inner Mongolia. *Int. Geol. Rev.* **2013**, *55*, 1029–1048. [[CrossRef](#)]
56. Woodhead, J.D.; Eggins, S.M.; Johnson, R.W. Magma Genesis in the New Britain Island Arc: Further Insights into Melting and Mass Transfer Processes. *J. Petrol.* **1998**, *39*, 1641–1668. [[CrossRef](#)]
57. Goswami, T.K. Subduction related magmatic constraints from the REE pattern in the Lohit Batholith, Arunachal Pradesh, India. *Geosciences* **2013**, *3*, 128–141.
58. Gou, J. Geochronology, Petrogenesis and Tectonic Setting of Mesozoic Volcanic Rocks, Southern Manzhouli. Ph.D. Dissertation, Jilin University, Changchun, China, 2013; pp. 1–89.
59. Defant, M.J.; Drummond, M.S. Derivation of some modern magmas by melting of young subducted lithosphere. *Nature* **1990**, *347*, 662–665. [[CrossRef](#)]
60. Wang, Z.H. The Mesozoic Early Cenozoic Tectono Magmatic Evolution of the Nadanhada Terrance. Ph.D. Dissertation, Jilin University, Changchun, China, 2017; pp. 1–100. (In Chinese with English Abstract)
61. Tang, J.; Xu, W.L.; Wang, F.; Wang, W.; Xu, M.J.; Zhang, Y.H. Geochronology and geochemistry of Early–Middle Triassic magmatism in the Erguna Massif, NE China: Constraints on the tectonic evolution of the Mongol–Okhotsk suture belt. *Lithos* **2014**, *184–187*, 1–16. [[CrossRef](#)]
62. Chen, Z.G.; Zhang, L.C.; Lu, B.Z.; Li, Z.L.; Wu, H.Y.; Xiang, P.; Huang, S.W. Geochronology and geochemistry of the Taipingchuan copper–molybdenum deposit in Inner Mongolia, and its geological significances. *Acta Petrol. Sin.* **2010**, *26*, 1437–1449. (In Chinese with English Abstract) [[CrossRef](#)]
63. Chen, Z.G.; Zhang, L.C.; Wan, B.; Zhang, Y.B.; Wu, H.Y. Geochemistry and geological significances of ore-forming porphyry with low Sr and Yb value in Wunugetushan copper–molybdenum deposit, Inner Mongolia. *Acta Petrol. Sin.* **2008**, *24*, 115–128. (In Chinese with English Abstract)
64. Zhao, Q.; Xiao, R.G.; Zhang, D.H.; Wang, J.P.; Zhang, Y.F.; Li, P.P. Petrogenesis and tectonic setting of ore-associated intrusive rocks in the Baiyinnuoer Zn–Pb deposit, southern Great Xing’an Range (NE China): Constraints from zircon U–Pb dating, geochemistry, and Sr–Nd–Pb isotopes. *Minerals* **2020**, *10*, 19. [[CrossRef](#)]
65. Gou, J.; Sun, D.Y.; Qin, Z. Late Jurassic–Early Cretaceous tectonic evolution of the Great Xing’an Range: Geochronological and geochemical evidence from granitoids and volcanic rocks in the Erguna Block, NE China. *Int. Geol. Rev.* **2019**, *61*, 1842–1863. [[CrossRef](#)]
66. Gou, J.; Sun, D.Y.; Ren, Y.S.; Hou, X.G.; Yang, D.G. Geochemical and Hf isotopic compositions of Late Triassic–Early Jurassic intrusions of the Erguna Block, Northeast China: Petrogenesis and tectonic implications. *Int. Geol. Rev.* **2017**, *59*, 347–367. [[CrossRef](#)]
67. Li, L.; Xiong, X.L.; Liu, X.C. Nb/Ta fractionation by amphibole in hydrous basaltic system: Implications for arc magma evolution and continental crust formation. *J. Petrol.* **2017**, *58*, 3–328.
68. Bailey, J.C. Geochemical criteria for a refined tectonic discrimination of orogenic and esites. *Chem. Geol.* **1981**, *32*, 139–154. [[CrossRef](#)]
69. Wood, D.A. The applications of a Th–Hf/3–Nb/12 diagram to problems of tectono magmatic classification and to establishing the nature of crustal contamination of basaltic lavas of the British Tertiary volcanic province. *Earth Planet. Sci. Lett.* **1998**, *50*, 11–30. [[CrossRef](#)]